Evaluating SAR Sea Ice Image Segmentation Using Edge-Preserving Region-Based MRFs

Xuezhi Yang[1], *Member*, *IEEE* and David A. Clausi[2], *Senior Member*, *IEEE*

[1]School of Computer and Information, Hefei University of Technology,
Hefei, Anhui, China, 230009

[2]Department of Systems Design Engineering, University of Waterloo,
Waterloo, Ontario, Canada, N2L 3G1

Abstract

This paper presents a new approach to sea ice segmentation in synthetic aperture radar (SAR) intensity images by combining an edge-preserving region (EPR)-based representation with region-level MRF models. To construct the EPR-based representation of a SAR image, edge strength is measured using instantaneous coefficient of variation (ICOV) upon which the watershed algorithm is applied to partition the image into primitive regions. In addition, two new metrics for quantitative assessment of region characteristics (region accuracy and region redundancy) are defined and used for parameter estimation in the ICOV extraction process towards desired region characteristics. In combination with a region-level MRF, the EPR-based representation facilitates the segmentation process by largely reducing the search space of optimization process and improving parameter estimation of feature model, leading to considerable computational savings and less probability of false segmentation. The proposed segmentation method has been evaluated using a synthetic sea ice image corrupted with varying levels of speckle noise as well as real SAR sea ice images. Relative to the existing region-level MRF-based methods, testing results have demonstrated that our proposed method substantially improves the segmentation accuracy at high speckle noise and achieves on average 29% reduction of computational time.

Index Terms — synthetic aperture radar (SAR), sea ice classification, Markov random field (MRF), instantaneous coefficient of variation, watersheds.

I. INTRODUCTION

Sea ice information is essential to the safety and efficiency of ship navigation in ice-infested regions [1]. Sea ice in polar regions also plays an important role in climate research, and receives considerable attention in recent years due to the increasing severity of global warming [2]. Spaceborne synthetic aperture radar (SAR), such as that carried by the Canadian satellites RADARSAT-1/2, provides an efficient method to monitor sea ice conditions especially for inaccessible regions. Manual processing of the large amount of SAR images is labor intensive and time consuming, while the labeling results by ice analysts have limited resolution and accuracy. The use of automated computer vision techniques is hence a desirable means to SAR image interpretation.
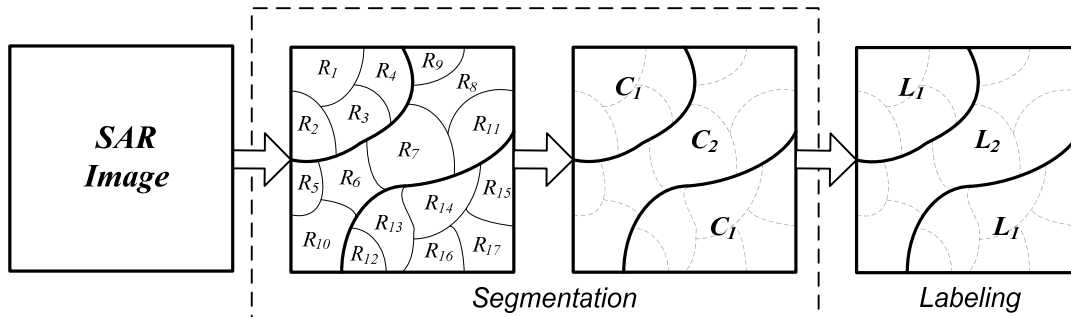
Fig. 1. A hierarchical approach to automated interpretation of SAR sea ice imagery

Automated SAR sea ice interpretation can be implemented in a hierarchical way with two major parts: segmentation and labeling, as illustrated in Fig. 1. Sea ice image segmentation first partitions a SAR image into disjoint primitive regions ($\{R_i\}$) in terms of local homogeneity with respect to intensity and texture. A relational graph built on the regions is termed region-based representation in this paper. On the region-based

representation, the segmentation process further groups regions ($\{R_i\}$) into a given number of region cluster ($\{C_j\}$), offering a high level description of SAR images. By incorporating expert knowledge of sea ice, the labeling process categorizes region clusters ($\{C_j\}$) into sea ice types ($\{L_j\}$) according to the definition by WOM [3] which includes: *new ice*, *grey*, *grey-white*, *thin first-year*, *medium first-year*, *thick first-year*, *old ice* and *open water*.

In this paper, we present an efficient solution to the segmentation of SAR sea ice images by using Markov random field (MRF) models.

A. MRF Approach to SAR Sea Ice Image Segmentation

Various methods have been proposed for SAR sea ice image segmentation, including thresholding [4] or clustering approaches [5],[6], hybrid approaches combining edge detection and region merging [7],[8], and MRF-based approaches [9],[10],[11],[12],[13],[14]. The MRF model [16] is capable of characterizing image structure by modeling contextual dependencies in images and has been widely adopted for the analysis of various types of remote sensing imagery [17],[18],[19],[20],[21]. Under the Bayesian framework, the MRF context model can be combined with a feature model to form a maximum *a posteriori* (MAP)-MRF framework, offering a mathematically sound way to solve image segmentation problem [16]. The usefulness of MRF model for SAR sea ice image segmentation has been studied in a number of applications. Deng and Clausi [9] proposed a new MRF model for the segmentation of

SAR sea ice images, where improved segmentation accuracy was obtained by introducing an adaptive weighting scheme for appropriate interactions between the feature model and the MRF model. This adaptive MRF model was later used by Maillard and Clausi [10], in combination with the extraction of egg-code-map-based sea ice information, to offer a cognitive reasoning approach to sea ice segmentation and labeling. Rather than applying MRF models on pixel-level, a region adjacency graph (RAG) representation of a SAR image was first constructed based on the watershed segmentation, and region-level MRF models was then applied for the segmentation of sea ice images [11],[12],[13],[14],[15]. Furthermore, edge strength between regions was incorporated into MRF models instead of the commonly used multi-level logistic (MLL) model [14], leading to better adaptability to non-stationary of SAR images.

B. Motivation and Objectives

Though various improvements have been made, the MRF-based methods still suffers difficulties in seeking accurate segmentation of SAR sea ice images in a computationally efficient manner. For MRF defined over pixels of SAR images which are normally of large size, the corresponding huge search space makes the optimization process computationally expensive, limiting the practical use of this segmentation method. In addition, the optimization process is prone to be trapped in local minima due to the disturbance of the inherent speckle noise. As an alternative to pixel-level MRF, an image can be initially segmented into disjoint regions upon which a region-level MRF [14],[22],

5

[23],[24] is applied to model spatial contexts between regions. In contrast to pixel-level MRF, MRF at region-level can gain considerable computational savings due to the much reduced search space, while the segmentation accuracy depends on characteristics of underlying region-based image representation, e.g., misplacements between region boundaries and actual object edges.

The existing region-based representations are normally constructed by applying watershed transform on SAR images [11],[12],[13],[14],[15],[22],[23]. These representations have a large number of segments due to speckle noise and feature variations, posing obstacles to region-level MRF-based segmentation with respect to both accuracy and computational efficiency. To overcome the problems, the impact of speckle noise and feature variations should be reduced in forming a region-based representation.

In this paper, we propose a new approach to sea ice segmentation in SAR intensity imagery by combining an edge-preserving region (EPR)-based representation with region-level MRF models. The EPR-based representation gives an initial segmentation of SAR images in the form of primitive regions, with the goal of efficiently suppressing oversegmentation within objects while accurately locating region boundaries at object edges. To achieve this goal, object edges and within-object homogeneity in SAR images are first characterized by instantaneous coefficient of variation (ICOV) derived using the speckle reduction anisotropic diffusion (SRAD) algorithm [27], which has the distinctive advantages of detecting edges in the presence of speckle noise [28]. The watershed algorithm [31] is further applied to partition the image into disjoint regions. In contrast to

the previous ICOV-based segmentation algorithm [29], our scheme aims at a segmentation result more appropriate for a combination with region-level MRF models towards segmentation purpose. Specifically, two new metrics for quantitative assessment of region characteristics (*region accuracy* and *region redundancy*) are defined and used for parameter estimation in the ICOV extraction process.

Combined with the EPR-based representation, the region-level MRF approach to SAR image segmentation is facilitated in the following two aspects:

First, the segmentation process is largely accelerated. In contrast to existing region-based representations, the EPR-based representation has much fewer regions which correspondingly narrows down the search space associated with the optimization process.

Second, the segmentation accuracy is improved over existing region-based representations. By alleviating speckle impacts on the segmentation, the EPR-based representation has much larger regions with boundaries positioning at object edges. In this manner, feature statistics of regions are less sensitive to speckle noise which leads to more accurate estimate of feature model parameters, and consequently reduces the probability of false segmentation.

In the next section, MRF model-based image segmentation is briefly introduced. The EPR-based representation of SAR images and its combination with region-level MRFs are then presented in Section III. Definition of region characteristic metrics and its use for parameter estimation of the ICOV extraction process are described Section IV, followed

by evaluations of the proposed method in Section V. This paper is concluded in Section VI.

II. MRF MODEL BASED SAR IMAGE SEGMENTATION

A. Traditional MAP-MRF Framework

Under the Bayesian framework, the image segmentation problem can be formulated as a MAP estimate [16]

$$C^* = \arg\max_C P(C|f) = \arg\max_C p(f|C)P(C), \tag{1}$$

where $P(C|f)$ denotes the posterior probability of the class label configuration C given the image feature f, $p(f|C)$ is the conditional probability distribution given the configuration C, referred to as the feature model, and $P(C)$ is the prior probability of the configuration C, referred to as the spatial context model.

For pixels of single- or multi-look SAR intensity images, the feature model follows a Gamma distribution. Assuming the spatial context model takes a MLL MRF model with pairwise cliques [16], the MAP-MRF solution to SAR image segmentation can be obtained by minimizing an objective function as follows [9]:

$$\arg\min_{\{c_s, s \in S\}} \left\{ \sum_{s \in S} \left\{ \frac{L}{\mu_{c_s}} f_s - (L-1)\log(f_s) + L\log(\mu_{c_s}) \right\} + \alpha \sum_{\langle s,k \rangle \in Q} U(c_s, c_k) \right\}, \tag{2}$$

where $S=\{s=(h,w) \mid 1 \leqq h \leqq M, 1 \leqq w \leqq N\}$ denotes a rectangular lattice for an image of size $M \times N$. c_s denotes the class label at site s, taking a value from the class label set $\{1,\ldots,n\}$ where n is the number of class labels in the segmented image and assumed to be

8

known *a priori*. L denotes the number of looks of the SAR image. f_s denotes intensity value at site s, and μ_{c_s} denote the mean pixel intensity of class c_s. The term α is a weighting parameter balancing the contributions of the feature and spatial context models. $<s, k>$ denotes one pair-site clique of the neighboring sites s and k, and Q denotes the set of all pair-site cliques on S. $U(c_s, c_k)$ is the pair-site clique energy whose form for the MLL model is

$$U\left(c_s, c_k\right) = \begin{cases} 1 & if \quad c_s \neq c_k \\ 0 & otherwise \end{cases}.$$ (3)

To minimize the objective function in (2), combinatorial optimization method such as the simulated annealing [16] can be used.

B. Region-Level MRF

Instead of the pixel-level definition, the MRF model can be applied to region-level of an image by modeling the spatial context over constituent regions [16],[25],[26]. The regions are homogeneous with respect to intensity feature and can be obtained by employing an initial segmentation process, e.g., the watershed transform. In contrast to the pixel-level MRF, label configurations of the region-level MRF are changed on regions instead of pixels, and the associated objective function is adapted from (2) as

$$\arg \min_{\{c_r, r \in S\}} \left\{ \sum_{r \in S} \sum_{s \in r} \left\{ \frac{L}{\mu_{c_r}} f_s - (L-1)\log(f_s) + L\log\left(\mu_{c_r}\right) \right\} + \alpha \sum_{\langle r,k \rangle \in Q_R} U\left(c_r, c_k\right) \right\},$$ (4)

where r denotes a region of pixels and the disjoint union of r constitute the image S. c_r denotes the class label of region r and μ_{c_r} denotes the mean pixel intensity of class c_r.
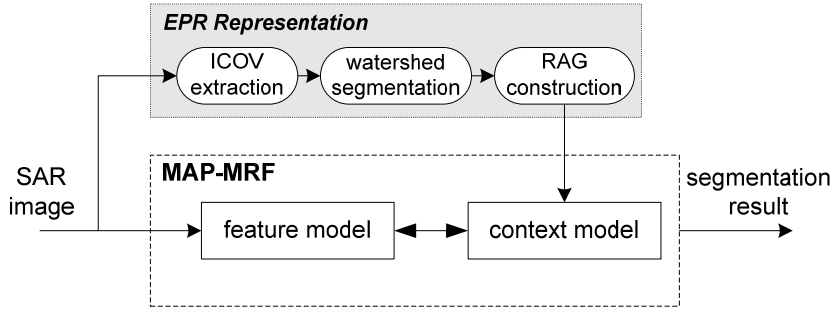
Figure 2. An edge-preserving region (EPR)-based MRF model for SAR sea ice
image segmentation

$<r, k>$ denotes one pair-region clique of the neighboring regions s and k, and Q_R denotes

the set of all pair-region cliques on S.

III. THE EDGE-PRESERVING REGION (EPR)-BASED MRF FOR SAR SEA ICE IMAGE

SEGMENTATION

The proposed segmentation scheme is illustrated in Fig. 2. In the MAP-MRF

framework, the original SAR image is fed into the feature model while a combination of

an EPR-based representation of the SAR image and a region-level MRF model is used as

the spatial context model. To facilitate the region-level MRF approach to SAR image

segmentation, the underlying region-based representation is expected to characterize

image contents in following two aspects:

a) *Region boundaries should be accurately located at object edges.* Deviations

between object edges and region boundaries cause segmentation error which cannot be

corrected by the MRF model. On the other hand, the deviations also cause bias in

parameter estimate of the feature model and further affect the segmentation accuracy.

b) *Oversegmentation within homogeneous objects should be minimized.* The degree of oversegmentation is proportional to the size of search space in optimization process and hence the computational burden of segmentation process. In the case of extensive oversegmentation, feature statistics of numerous tiny regions are dominated by speckle noise and feature variations which can lead to erroneous segmentation.

To build region-based representations with above desirable characteristics, object edges and homogeneity within objects need to be enhanced which relies on an accurate detection of edges. A large number of algorithms have been developed for detecting edges in SAR images, e.g., the ratio-based detectors with constant false alarm rate [32][33][34]. However, these local window-based detectors have limited capability in describing within-object homogeneity which is hence not suitable for reducing oversegmentation of region-based presentations. In this work, the ICOV edge detector [28] is adopted for its accurate location of object edges in the presence of speckle noise and feature variations, as well as its multiscale nature appropriate for revealing within-object homogeneity. By using the ICOV, the so-called edge-preserving region (EPR)-based representation is constructed for SAR images in three steps as illustrated in Fig. 2. The ICOV edge strength map of a SAR image is first extracted by using the SRAD algorithm, which is then used by the watershed transform to decompose the image into primitive regions, upon which a RAG is constructed to form a region-based representation.

A.   ICOV Extraction Using the SRAD Algorithm

Let *I* denote the intensity of a SAR image, the ICOV edge strength is computed as

$$q = \left\{ \frac{\frac{1}{2}\left(\frac{|\nabla I|}{I}\right)^2 + \frac{1}{16}\left(\frac{\nabla^2 I}{I}\right)^2}{\left[1+\frac{1}{4}\left(\frac{\nabla^2 I}{I}\right)\right]^2} \right\}^{1/2} \tag{5}$$

where q denotes the ICOV, $|\nabla|$ is the magnitude of gradient and ∇^2 is the Laplacian operator. The ICOV is a combination of normalized gradient operator and normalized Laplacian operator, which gives consistent measures of edge strength in areas of different radiometric intensities by taking into account the multiplicative nature of speckle noise [28]. The ICOV can be iteratively refined by using the SRAD algorithm which reduces the impact of speckle noise and generates a multiscale edge measures of SAR images

The SRAD algorithm provides a partial differential equation (PDE) approach to speckle reduction of SAR images by introducing anisotropic diffusion [30] into the conventional Lee filter [35]. Starting from an original SAR image I_0, the SRAD algorithm iteratively updates filtering result $I(t)$ according to the following PDE:

$$\begin{cases} \frac{\partial I(t)}{\partial t} = div[c(q)\nabla I(t)], \\ \quad\quad I(0) = I_0 \end{cases} \tag{6}$$

where t is the time variable, *div* the divergence operator. $c(q)$ is the diffusion coefficient defined on the ICOV q

12

$$c(q) = \frac{1}{1 + \frac{q^2 - q_0^2}{q_0^2(1 + q_0^2)}}, \tag{7}$$

where q_0 is a function indicating intensity fluctuations in homogeneous regions caused by speckle noise which is then used by the $c(q)$ to identify edges from homogeneous regions. The q_0 can be estimated by

$$q_0 = \frac{\sigma(I(t))}{\mu(I(t))}, \tag{8}$$

where $\mu(I(t))$ and $\sigma(I(t))$ are the mean and standard deviation of $I(t)$ over a homogeneous local window respectively. It should be noted that q, q_0, and $c(q)$ need to be updated at each iteration of the SRAD algorithm while the time variable t in these functions are omitted throughout the paper for clarity.

By incorporating the ICOV q into the diffusion coefficient $c(q)$, edge information can be used to guide the PDE process by encouraging isotropic diffusion in homogeneous regions while only allowing directed diffusion along edges. As a consequence, speckle noise in homogeneous regions as well as at edges can be efficiently reduced. Based on the despeckling result $I(t)$, the ICOV can be computed for a more accurate measure of edge strength. In order for a successful detection of object boundaries, it should also be noted that the within-object ICOV should be smaller than that at object boundaries. However, this may not hold in the cases of heavy speckle noise or highly textured areas where within-object intensity variations are large. Therefore, the ICOV is more

appropriate for detecting object boundaries between homogeneous regions where speckle noise can be efficiently reduced and feature variations are minor.

B. The Watershed Algorithm

The watershed algorithm [31] is a popular morphological tool for image segmentation. It uses a drainage pattern of simulated rainfall to partition an image into disjoint regions called catchment basins separated by watershed lines. Based on edge strength measures of an image, the watershed algorithm combines identification of discontinuities and a region growing technique to reveal topological structure of the image, which detects object edges at boundaries of watershed regions. As a distinct advantage over other edge detection methods, object edges extracted by the watershed algorithm are always connected/closed and one-pixel width, which can be used for segmentation either by tracking the object boundaries or using region-based methods. In this work, based on the ICOV edge strength, we adopt immersion simulations algorithm [31] to compute watersheds of a SAR image.

C. The RAG Representation

To facilitate the use of the MRF model on region level, a region adjacency graph (RAG) [16] is then constructed to represent the watershed regions and their context relationships in the segmented image. The RAG provides an efficient structure for describing the content of an image by using a set of nodes and arcs, where each node
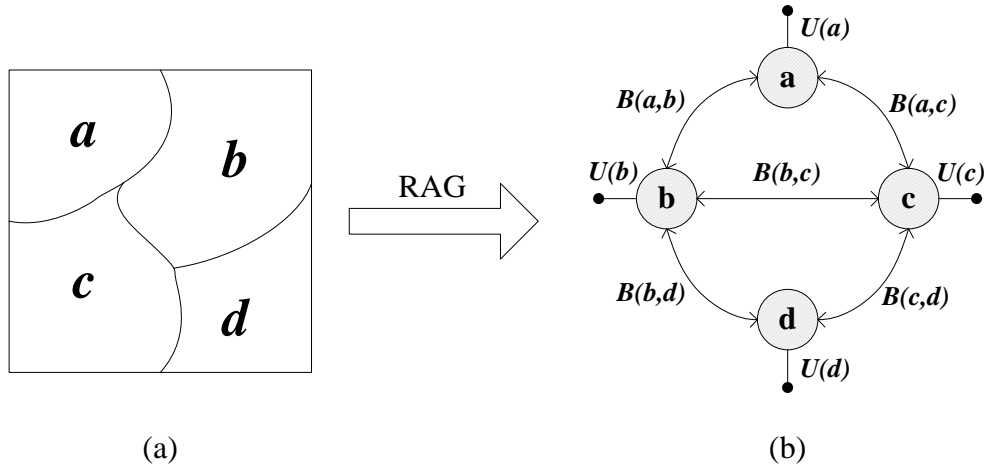
Figure 3. (a) A watershed segmentation, (b) the corresponding RAG representation, where $U(\cdot)$ and $B(\cdot,\cdot)$ denote unary properties of nodes and binary relationships between nodes respectively

represents a region while the adjacency between regions is represented by an arc. Fig. 3 illustrates an example of watershed segmentation and its associated RAG representation.

IV. EVALUATING CHARACTERISTICS OF THE EPR-BASED REPRESENTATION

In this section, we develop two quantitative metrics for objective assessment of characteristics of region-based SAR image representations, which are then used for the estimation of appropriate parameters in the ICOV extraction process towards desired region characteristics for SAR sea ice image segmentation. In addition, advantages of the EPR-based representation over other region-based representations are investigated in terms of the region characteristic metrics.

A. Objective Assessment of Characteristics of Region-Based Representations

15

Two region characteristic metrics are defined in accordance with the purpose of locating region boundaries at object edges while minimizing oversegmentation within objects. Definition of the metrics involves two images. One is a noise-free reference image where true object edges can be extracted. The other one is a noisy image by adding speckle noise to the noise-free image, upon which a region-based representation is generated.

- Region accuracy (R_a)

R_a is used to measure the accuracy of locating object edges by boundaries of the region-based representation

$$R_a = \frac{1}{N_e} \sum_{i=1}^{N_e} \frac{1}{1+d_i^2} \tag{9}$$

where N_e indicates the number of true edge points detected in the noise-free image. d_i^2 denotes the Euclidean distance between the ith true edge point and its nearest boundary point in the region-based representation. Ranging from 0 to 1, R_a reaches its maximum when all the edge points are covered by region boundaries.

- Region redundancy (R_r)

R_r indicates the degree of oversegmentation within objects by measuring the redundancy of a region-based representation

$$R_r = 1 - \frac{N_e}{N_{\partial R}} \tag{10}$$

where $N_{\partial R}$ is the number of boundary points in the region-based representation. R_r falls into the range of 1-N_e to 1-N_e/N_I where N_I denotes the number of image pixels. For a given number of object edge points N_e, smaller R_r means less oversegmentation.

The two region characteristics are closely related to the final segmentation performance. Segmentation accuracy depends on both region accuracy and region redundancy while segmentation time is proportional to region redundancy. The superiority between the region accuracy and the region redundancy actually depends on the major concern of the segmentation (accuracy or time) and normally a tradeoff between them has to be made.

B. Parameter Estimation of the ICOV Extraction Process Based on Region Characteristic Metrics

To generate the ICOV edge strength of a SAR image, the SRAD algorithm needs to determine the speckle level function q_0 in (7). The speckle level function q_0 is used to discriminate the response of speckle noise at each iteration of the diffusion process which is hence closely related to the consequent region-based representations. If q_0 is too small, speckle noise cannot be efficiently suppressed and hence oversegmentation reduction is very limited. On the other hand, if q_0 is too large, deviations between region boundaries and objects edges may become serious. In [29], q_0 is computed on a homogeneous region selected in the SAR image as in (8) which may limit its practical use. In this work, q_0 is assumed to take a form of exponential decay [27]
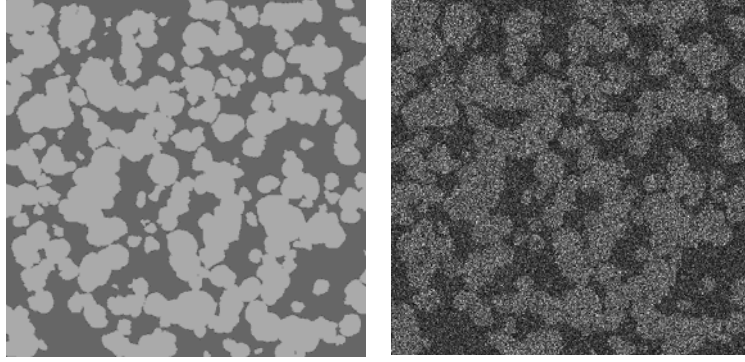
(a) A synthetic sea ice image.　　(b) A simulated SAR image
　　　　　　　　　　　　　　　with 2-look speckle noise

Figure 4. A simulated SAR sea ice image

$$q_0 = \frac{1}{\sqrt{L}} \exp(-kt) \tag{11}$$

where L denotes the nominal number of looks of the SAR image, k is a scale parameter, and t is the time variable. To determine an appropriate value of the speckle level function specifically for SAR sea ice images, impact of the scale parameter k on region characteristics is experimentally studied by using the metrics R_a and R_r.

Fig. 4a shows a synthetic sea ice image which contains brighter ice floes of varying shapes and darker open water. The image is corrupted by 2-look speckle noise in intensity format and produces a simulated SAR sea ice image as shown in Fig. 4b. A set of EPR-based representations of Fig. 4b are generated by using the SRAD algorithm with different scale parameter k ranging from 1/2 to 1/20. Fig. 5 illustrates the evolution of region characteristic metrics R_a and R_r in the SRAD process, where the scale parameter k takes the value of 1/4, 1/6, 1/8 and 1/10 respectively. As indicated by the figure, region redundancy (dashed lines) is gradually reduced along with the diffusion process while region accuracy (solid lines) decreases at the same time. A comparison of region
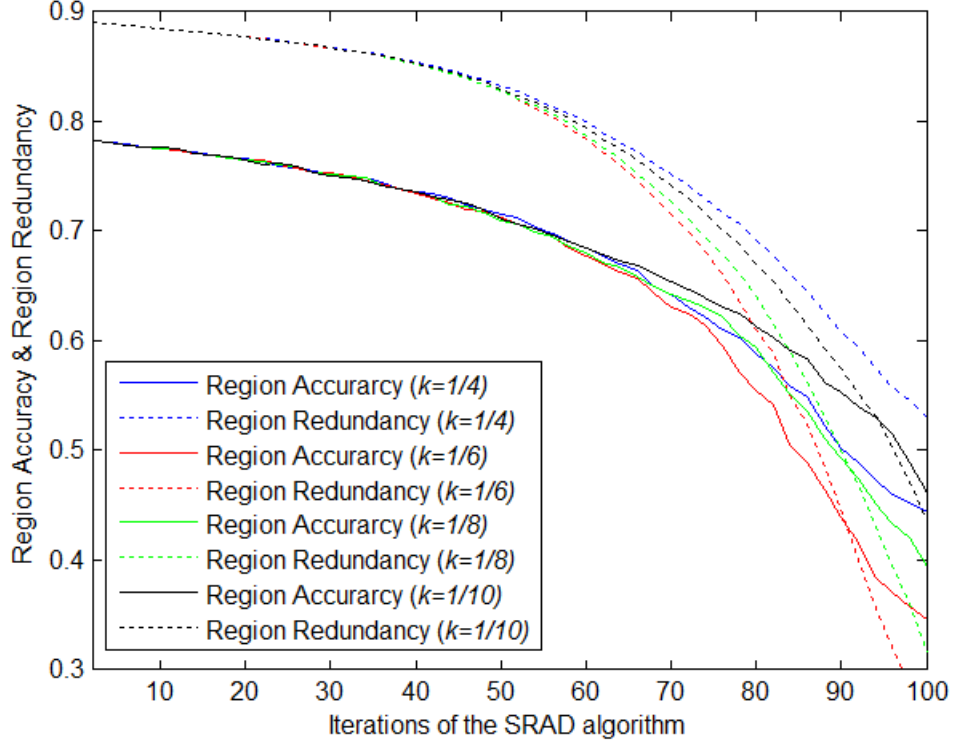
Figure 5. Impacts of the scale parameter k on region characteristics

characteristics at around iteration 55 demonstrates the advantages of $k=1/6$ over the other values, where different k lead to almost the same region accuracy while $k=1/6$ has the least region redundancy.

C. Comparisons of the EPR-Based Representation to Other Region-Based Representations

Advantages of the EPR-based representation are studied based on the simulated SAR image Fig. 4b, by comparing watershed segmentation on ICOV edge strength with other types of edge strength measures of SAR images, which include gradients of SAR images, gradients of despeckling results of SAR images (Lee filter [35], enhanced Lee filter [36]),
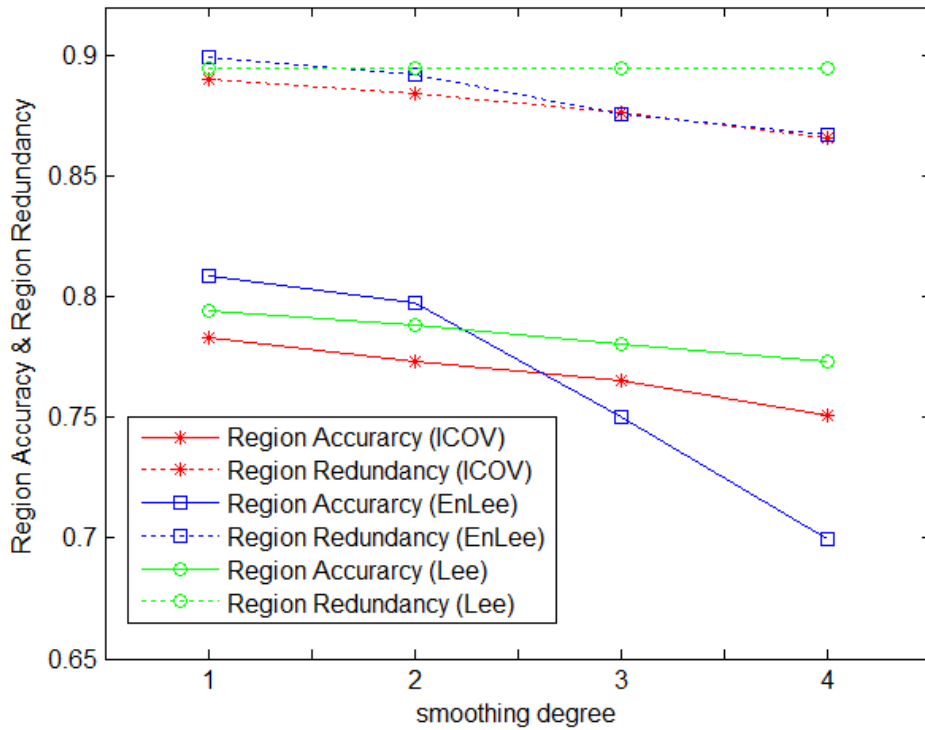
Figure 6. Region characteristics of watershed segmentation on ICOV edge strength and gradients of despeckling results

and ratio-based edge strength with constant false alarm rate (ratio of averages [32], ratio detector [33]).

The first comparison is between watershed segmentation on ICOV edge strength and gradients of despeckling results using the Lee filter and the enhance Lee filter respectively. These three filters are studied by adjusting their parameters (such as the q_0 in the SRAD filter) to generating filtering results of Fig. 4b with increasing smoothing degrees. Characteristics of the corresponding region-based representations at four different smoothing degrees are shown in Fig. 6. Along with the increase of smoothing degree, it can be seen the Lee filter results in very limited reduction on region redundancy

Table I. Region characteristics of watershed segmentation on ICOV edge strength and ratio-based edge strength

	Region Accuracy	Region Redundancy
ICOV	0.765	0.876
Ratio detector	0.746	0.878
Ratio of averages	0.762	0.881

while region accuracy keeps decreasing. On the other hand, the enhanced Lee filter is more capable of reducing region redundancy. The superiority of the EPR representation over the enhanced Lee filter-based region representation is clearly demonstrated at the third and fourth smoothing degrees, where better region accuracy while almost the same region redundancy are obtained.

Further comparison is between watershed segmentation on ICOV edge strength and ratio-based edge strength with constant false alarm rate. Characteristics of regions generated by using the ICOV, the ratio of averages and the ratio detector are listed in Table I where the size of window for extracting the ratio-based edge strength is 9×9. As shown in the table, the ICOV outperforms the ratio-based edge strength on both region accuracy and region redundancy which indicates the advantages of ICOV on measuring edge strength in the presence of speckle noise.

V. SEGMENTATION TESTING AND RESULTS

A. Testing Setup

Sea ice segmentation in SAR intensity images using the EPR-based MRF model (EPR-MRF) is tested and compared to the use of the traditional pixel-level MRF model as well as two other region-level MRF models. The first one is a noisy region(NR)-based MRF model (NR-MRF), where the noisy regions are generated by watershed segmentation on gradients of SAR images. The second one is the recently developed IRGS (iterative region growing using semantics) algorithm [13],[14] which is also a noisy region-based MRF approach to image segmentation.

In the objective function (2) or (4) of MRF-based image segmentation, the weighting parameter α need to be determined. For the pixel-level MRF, an adaptive weighting scheme used for SAR sea ice image segmentation [9] is adopted where the α is fixed to be 1 and the feature model is weighted by $80*0.98^n+1$ at the nth iteration of the optimization process. It is worth noting that the weighting scheme balancing the feature model and the spatial context model has a considerable impact on the segmentation performance of pixel-level MRFs. Other weighting schemes, such as the one used in [38] which takes into account image characteristics, may further improve the segmentation accuracy while increase the computational time as well. For the region-level MRF, the α is empirically determined as 0.4 for simulated SAR sea ice images which demonstrates better segmentation result than the other values. The real SAR sea ice images have much more complicated structures than the simulated ones, and an appropriate value of α is empirically selected to be 3.0. The simulated annealing algorithm [16] is used to iteratively minimize the objective function, where the temperature T is decreased with the

iteration n as $T(n) = 0.98^{n}$, and the number of iterations is set up as 300. Parameter estimation of the IRGS algorithm is the same as its original work [14].

Method performance is evaluated in terms of the segmentation accuracy and computational time. Overall accuracy and kappa are used to measure segmentation accuracy. Overall accuracy refers to the percentage of pixels correctly classified. In addition, the kappa coefficient is applied to measure the performance in terms of the segmentation agreement [37]. The kappa coefficient has a range of -1 to 1, where a value close to 1 indicates better agreement. In general, a kappa coefficient greater than 0.8 indicates a strong agreement.

B. Segmentation Results

- *Simulated SAR Sea Ice Intensity Images*

The segmentation method is first evaluated using a synthetic sea ice image shown in Fig. 4a. The image is corrupted by multiplying simulated speckle noise at six levels with the corresponding number of looks (L): 1, 2, 3, 4, 8, 16.

Table II lists the segmentation accuracy of the synthetic image (Fig. 4a) across different speckle noise levels. For the single-look SAR image, the pixel-level MRF results in poor segmentation results since the heavy speckle noise causes estimates of feature model parameters seriously deviate from their true values. By using the region-level MRF, the segmentation accuracy substantially increases since the impact of speckle noise on regions are much less than that on pixels. When the noise level

Table II. Segmentation results (overall accuracy / kappa) for Fig.
4a corrupted with varying levels of speckle noise.

L	Pixel-level MRF	Region-level MRF		
		IRGS	NR-MRF	EPR-MRF
16	**98.7/0.974**	98.2/0.964	98.1/0.961	98.4/0.967
8	**97.7/0.954**	96.6/0.931	96.5/0.930	97.3/0.945
4	**96.3/0.926**	93.7/0.872	94.4/0.886	95.5/0.908
3	**95.5/0.909**	91.5/0.828	93.0/0.857	94.5/0.888
2	91.1/0.815	88.0/0.759	90.8/0.811	**92.7/0.849**
1	57.3/0.000	75.1/0.520	82.4/0.640	**88.1/0.751**
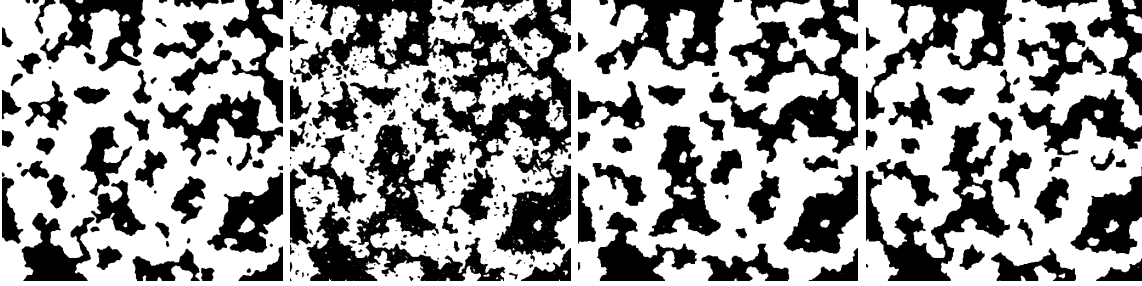
(a) the pixel-level MRF   (b) the IRGS   (c) the NR-MRF   (d) the EPR-MRF

Figure 7. Segmentation of the simulated 2-look SAR sea ice image (Fig. 4b) by using
pixel-level MRF and region-level MRF (IRGS, NR-MRF, EPR-MRF)

decreases to $L>3$, the pixel-level MRF produces more accurate segmentation results

than the region-level MRF. For the three types of region-level MRF, in contrast to the

use of noisy regions, it can be seen that the EPR-based MRF gains distinct

improvements over the NR-MRF and the IRGS at speckle levels from 1 to 16.

Specifically, increases on segmentation accuracy are proportional to the speckle level,

and the largest increase is at the highest noise level of single-look. The results clearly

indicate that the performance of region-level MRF model is closely related to the underlying region-based representation due to the presence of noise. Relative to the noisy regions, the EPR-based representation is more capable of revealing the local image structures in SAR images which facilitates the MRF model in dealing with heavy speckle noise.

An example of segmentation on the simulated 2-look SAR image (Fig. 4b) is shown in Fig. 7. In contrast to the pixel-level MRF (Fig. 7a), the NR-MRF (Fig. 7b) and the IRGS (Fig. 7c), the EPR-MRF (Fig. 7d) is more accurate in locating boundaries of ice floes and demonstrates an improved result with less false segmentation.

- *Real SAR Sea Ice Images*

The proposed segmentation method is applicable on single-channel, single- or multi-look SAR intensity data. Real SAR sea ice images used for evaluation are shown in Fig. 8, which were captured by RADARSAT-2 over LiaoDong Bay, China on January 14, 2009 in Quad-Polarization mode (HH, HV, VH, VV polarizations) with the resolution of 8m and the nominal number of looks is one. The images contain *grey ice*, *grey-white ice* as well as *open water* as indicated by the manual interpretation shown in Fig. 8e.

The segmentation task is to divide the image into three classes while without further labeling the results with sea ice types. Segmentation accuracy of the HH-, HV-, VH-, VV-polarized images using various MRF models are listed in Table III which takes the manual interpretation in Fig. 8e as the ground truth. The IRGS algorithm has much poorer segmentation accuracy than the other algorithms since it assumes a Gaussian
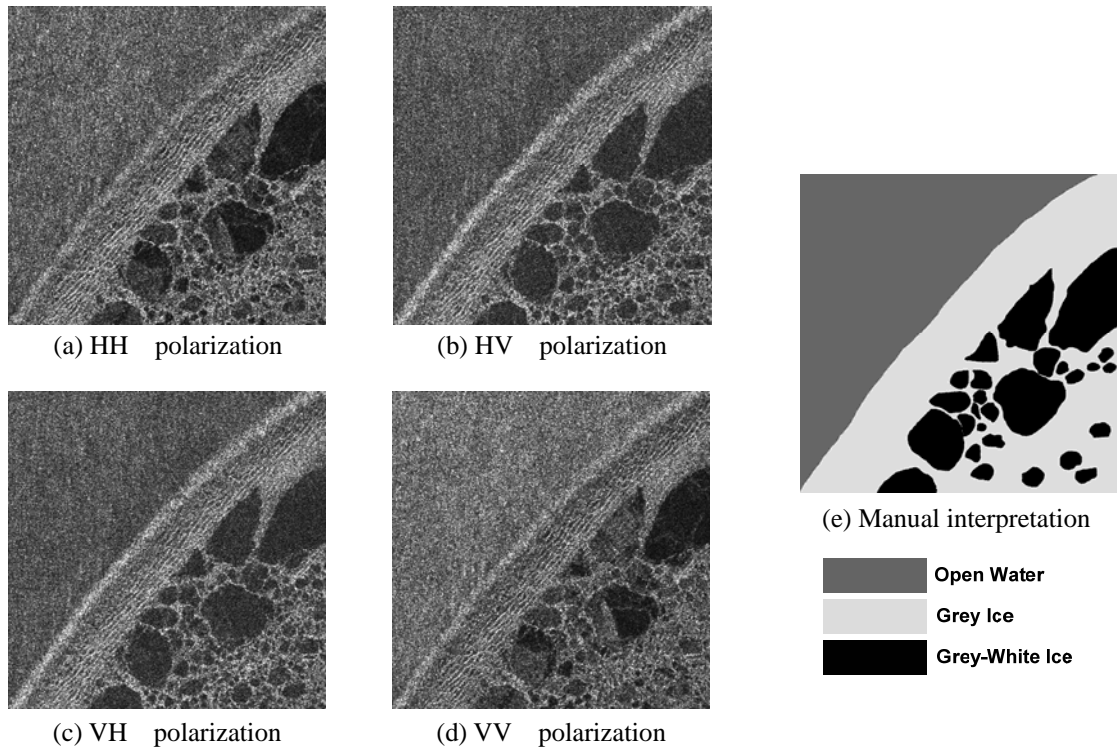
(a) HH   polarization

(b) HV   polarization

(c) VH   polarization

(d) VV   polarization

(e) Manual interpretation

Open Water
Grey Ice
Grey-White Ice

Figure 8. SAR sea ice images captured by RADARSAT-2 over LiaoDong Bay, China on January 14, 2009 in Quad-Polarization mode

Table III. Single-look segmentation results (overall accuracy / kappa) for Fig. 8a to 8d with HH, HV, VH and VV polarization.

Polarization	Pixel-level MRF	Region-level MRF		
		IRGS	NR-MRF	EPR-MRF
HH	62.7/0.436	56.2/0.312	73.1/0.578	**80.2/0.688**
HV	63.3/0.463	47.7/0.239	77.9/0.661	**86.8/0.795**
VH	65.0/0.475	47.8/0.245	73.5/0.595	**87.0/0.798**
VV	56.4/0.325	46.5/0.133	60.0/0.374	**63.1/0.416**

distribution of pixel values which is far from the actual exponential distribution at single-look. Relative to the pixel-level MRF, the two region-level MRF (the NR-MRF and the EPR-MRF) demonstrates improved segmentation accuracy and the EPR-MRF
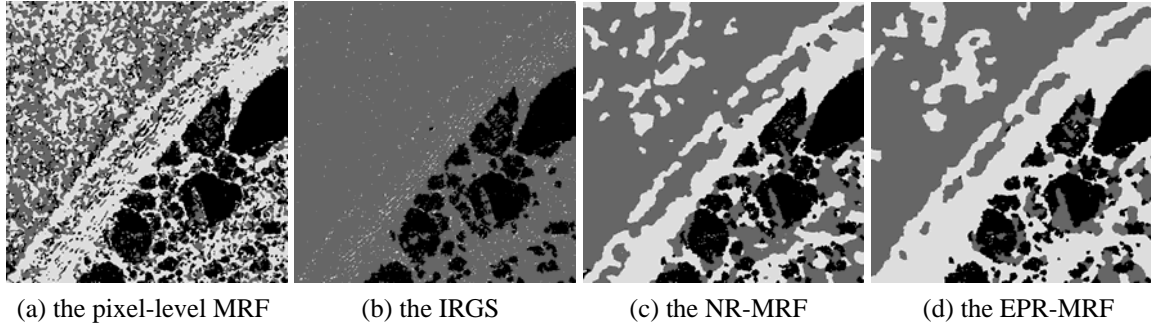
(a) the pixel-level MRF   (b) the IRGS   (c) the NR-MRF   (d) the EPR-MRF

Fig. 9. Segmentation of the *HH*-polarized SAR sea ice image (Fig. 8a).

(a) the pixel-level MRF   (b) the IRGS   (c) the NR-MRF   (d) the EPR-MRF
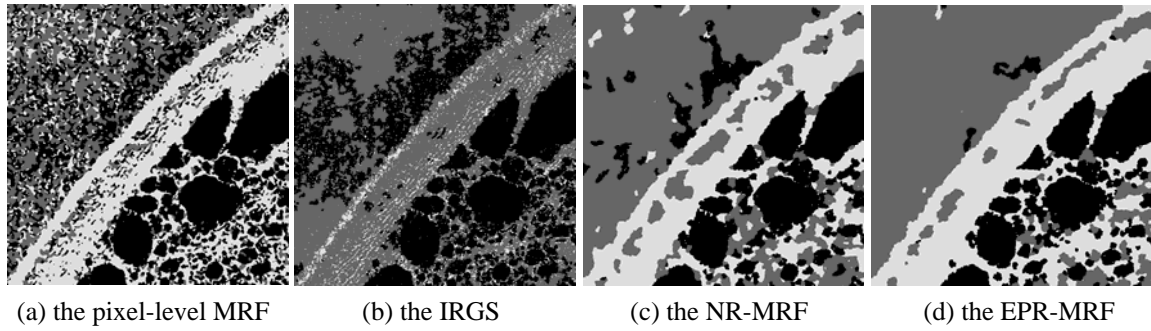
Fig. 10. Segmentation of the *HV*-polarized SAR sea ice image (Fig. 8b).

(a) the pixel-level MRF   (b) the IRGS   (c) the NR-MRF   (d) the EPR-MRF
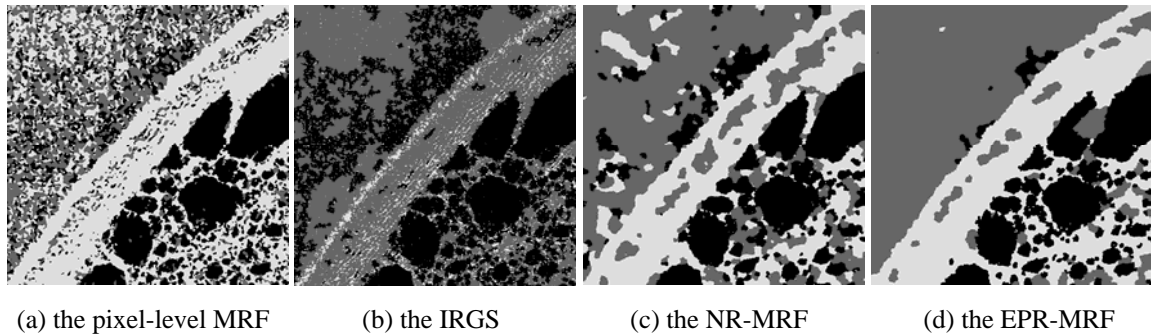
Fig. 11. Segmentation of the *VH*-polarized SAR sea ice image (Fig. 8c).

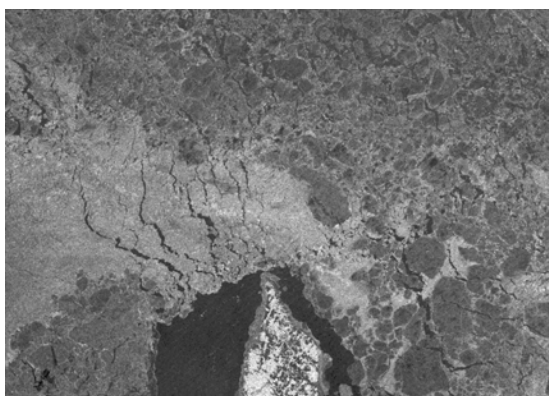(a) the pixel-level MRF   (b) the IRGS   (c) the NR-MRF   (d) the EPR-MRF
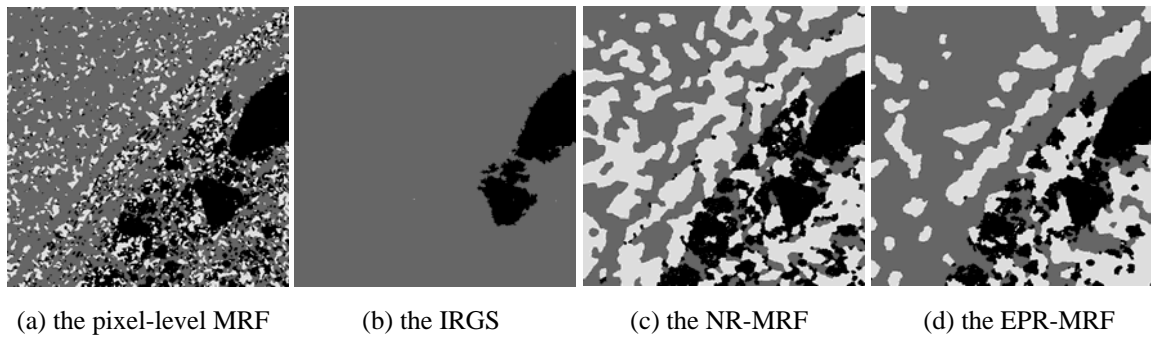
Figure 12. Segmentation of the *VV*-polarized SAR sea ice image (Fig. 8d).

achieves the best results across all the four polarization channels. Specifically in the case of HV and VH polarization, the kappa coefficients are largely increased from 0.23 or 0.24 (by the IRGS) to 0.79. Segmentation results of the HH-, HV-, VH-, VV-polarized images using the pixels-level MRF, the IRGS, the NR-MRF and the EPR-MRF are shown in Fig. 9 to Fig. 12. The results indicate that the pixel-level MRF and the IRGS are weak in discriminating the grey ice and the open water which have relatively small intensity differences. The advantages of the proposed EPR-MRF are clearly shown in Fig. 9d to Fig. 12d where efficient separations between the open water, the grey ice and the grey-white ice can be observed in the HV and the VH polarization (Fig. 10d and Fig. 11d).

Sea ice and open water exhibit varying intensity features in different polarization models and between-class differences fundamentally affect accuracy of segmentation methods. As shown in Fig. 8, intensity differences between grey ice and open water in the VV polarization are smaller than the other three polarizations and hence causes the worst accuracy for all the segmentation methods.

In our future work, the proposed method would be extended from single-polarization to multi-polarization to produce a fused segmentation map. For this purpose, the ICOV needs to be extended to a multi-variate form to deal with multi-polarization data which can then be used to generate a region-based representation. In addition, the MAP-MRF formulation should be adapted to multi-polarization data as well.
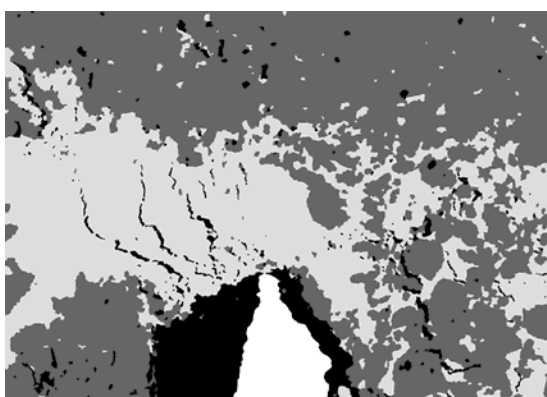
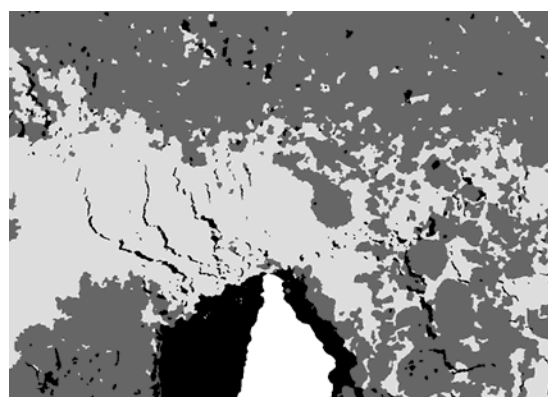(a) Original SAR image
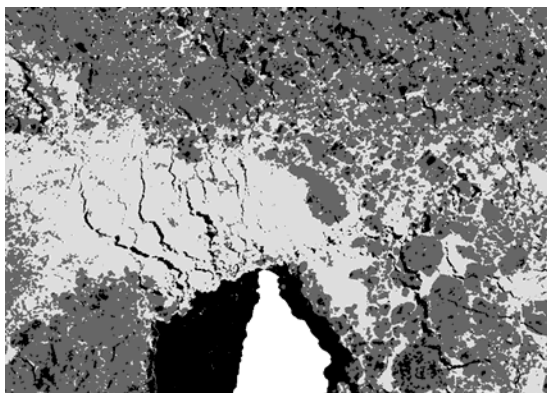
(b) Segmentation using the pixel-level MRF

(c) Segmentation using the IRGS

(d) Segmentation using the NR-MRF

(e) Segmentation using the EPR-MRF

Figure 13. Segmentation of a SAR image captured over Gulf of Saint Lawrence. White regions in (b)-(e) indicate the land, which is not included in the segmentation process.

The proposed method is further evaluated using a SAR sea ice image shown in Fig. 13a which was captured over Gulf of Saint Lawrence on Feb 20, 1998 by RADARSAT-1 in ScanSAR C-band mode. The image with the original resolution of 50m has been processed by Canadian Ice Service (CIS) using a 2×2 block average which reduced the resolution to 100m for operational use. The equivalent number of looks of the SAR image is approximately 11. At the bottom of the image is land surrounded by water. The land is not included in the segmentation and marked as white regions in Fig. 13b-13e. The bright area at the middle of the image is *grey ice*, inside which the narrow and dark cracks are called *leads*, which contain open water, and the rest of the dark regions are *grey-white ice*. The difficulty with the segmentation task is on the grey-white ice in the right of the image where the intensity feature exhibits large variations. Fig. 13b presents the segmentation result using the pixel-level MRF. The grey-white ice in the right of the image is over-segmented and part of the grey-white ice is falsely classified into the grey ice, which is primarily caused by the intra-object variations. Segmentation result using the region-level MRF are shown in Fig. 13c to Fig. 13e which have less oversegmentation in the grey-white ice and reduced false segmentation, indicating the region-level MRF is more capable of dealing with intra-object intensity variations. In such an example with a relatively low noise level, the EPR-MRF has not gain a better result over the IRGS.

C. Computational Time

Table IV. Number of regions in the NR-based representation and the
EPR-based representation for the testing SAR images

	Number of looks	Image size	The NR-based representation	The EPR-based representation	Reduction ratio
Fig. 4b	2	512×512	27349	11556	**57%**
Fig. 8a	1	1410×1410	104755	69957	**33%**
Fig. 8b	1	1410×1410	109791	72130	**34%**
Fig. 8c	1	1410×1410	117113	71473	**39%**
Fig. 8d	1	1410×1410	112641	71561	**36%**
Fig. 13a	11	1209×865	86405	28350	**67%**

For an image of size $M \times N$, the pixel-level MRF-based segmentation has a computational complexity of $O(MNJK)$, where J is the number of iterations in the optimization process and K is the number of classes in the image to be classified. For SAR sea ice images which are normally of large-size, the computational burden of the pixel-level MRF is obviously very heavy. The problem can be substantially alleviated by using the region-level MRF, whose computational complexity is reduced to $O(RJK)$ where R is the number of regions.

Table IV lists the number of regions in the NR-based representation and the EPR-based representation for testing SAR images with varying sizes and noise levels (Fig. 4b, Fig. 8a to 8d, Fig. 13a). In this table it can be seen that the EPR-based representation has significantly fewer regions compared to the NR-based representation with an average reduction ratio of 44.3%, indicating considerable computational savings.

Table V. Computational time for Segmenting the testing SAR
images (in seconds).

	Image size	Pixel-level MRF	Region-level MRF		
			IRGS	NR-MRF	EPR-MRF
Fig. 4b	512×512	61	26	22	**11**
Fig. 8a	1410×1410	724	103	84	**66**
Fig. 8b	1410×1410	745	90	86	**67**
Fig. 8c	1410×1410	749	96	90	**66**
Fig. 8d	1410×1410	761	116	86	**66**
Fig. 13a	1209×865	356	41	66	**28**

In specific, the reduction ratio of regions gained by the EPR-based representation is inversely proportional to the noise level which is around 35% at 1-look and increases to 67% at 11-look.

The segmentation algorithms are implemented with *C++* and run on a laptop with Dual-Core CPU @ 2.53GHz and 2GB memory. The computational time needed for the segmentation of several testing SAR images is list in Table V. The pixel-level MRF takes much more time than the region-level MRF on the segmentation due to the huge search space. In contrast to the NR-MRF and the IRGS, the EPR-MRF based on largely reduced regions further leads to on average 29% computation savings.

VI. CONCLUSIONS

In this paper, an efficient method for the segmentation of SAR sea ice imagery is proposed by applying region-level MRF models on the EPR-based representation. The segmentation performance of region-level MRFs is closely related to the characteristics of underlying region-based image representations. More specifically, the computational complexity is proportional to the degree of oversegmentation within homogeneous objects, while the segmentation accuracy depends on both the degree of oversegmentation and the deviations between object edges and region boundaries. The existing region-based representation has not properly taken into account the effect of speckle noise and feature variations which suffers serious oversegmentation and inaccurate location of object edges. The problem can be alleviated by using the ICOV for its accurate location of object edges in the presence of speckle noise as well as its multiscale nature appropriate for revealing within-object homogeneity. Our new scheme substantially improves the accuracy of region-level MRF approach to SAR sea ice image segmentation at high noise level of one-look. In addition, on average 29% computational time is reduced as well. For large-size SAR sea ice images, considerable computational savings obviously benefits the practical use of the segmentation method. Based on the segmentation results of the proposed method, further labeling of sea ice types can be achieved by using a clustering algorithm incorporating feature distributions of various types of sea ice.

Two region characteristic metrics, region accuracy and region redundancy, have been defined which can be used to guide parameter selection in forming a region-based

representation. In the future work, a new metric combining the two metrics would be studied for measuring region characteristics in a way consistent with the segmentation accuracy.

ACKNOWLEDGMENT

REFERENCES

[1] Canadian Ice Services [Online]. Available: http://ice-glaces.ec.gc.ca.

[2] D. Rothrock, Y. Yu and G. Maykut, "Thinning of the Arctic sea-ice cover", *Geophysical Research Letters*, vol. 26, no. 23, pp.3469-3472, 2000.

[3] World Meteorology Organization [Online]. Available: http://www.wmo.ch/index-en.html.

[4] D. Havercamp, L. K. Soh and C. Tsatsoulis, "A dynamic local thresholding technique for sea ice classification", *Proc. Int'l Geosci. and Remote Sensing Symp.*, vol. 2, pp. 638-640, 1993.

[5] L. K. Soh and C. Tsatsoulis, "Unsupervised segmentation of ERS and RADARSAT sea ice images using multiresolution peak detection and aggregated population equalization", *Int. J. Remote Sensing*, vol. 20, no. 15-16, pp. 3087-3109, 1999.

[6] D. A. Clausi and B. Yue, "Comparing co-occurrence probabilities and Markov random fields for texture analysis of SAR sea ice imagery", *IEEE Trans. Geosci. Remote Sensing*, vol. 42, no. 1, pp. 215-228, 2004.

[7] L. K. Soh, C. Tsatsoulis, D. Gineris and C. Bertoia, "ARKTOS: An intelligent system for SAR sea ice image classification", *IEEE Trans. Geosci Remote Sensing*, vol. 42, no. 1, pp. 229-248, 2004.

[8] Q. Yu and D. A. Clausi, "Combine local and global features for image segmentation using iterative classification and region merging ", *Proc. 2nd Canadian Conf. on Computer and Robot Vision*, pp. 579-586, 2005.

[9] H. Deng and D. A. Clausi, "Unsupervised segmentation of synthetic aperture radar sea ice imagery using a novel Markov random field model", *IEEE Trans. Geosci Remote Sensing*, vol. 43, no. 3, pp. 528-538, 2005.

[10] P. Maillard, D. A. Clausi and H. Deng, "Operational map-guided classification of SAR sea ice imagery", *IEEE Trans. Geosci Remote Sensing*, vol. 43, no. 2, pp. 2940-2951, 2005.

[11] W. Yang, C. He, Y. Cao, H. Sun and X. Xu, "Improved classification of SAR sea ice imagery based on segmentation", *Proc. Int'l Geosci. and Remote Sensing Symp.*, pp. 3727-3730, 2006.

[12] Q. Yu, "Automated SAR sea ice interpretation", *Ph.D. Thesis,* University of Waterloo*, 2006. Available: http://www.eng.uwaterloo.ca/~dclausi/students.html.

[13] Q. Yu and D. A. Clausi, "SAR sea-ice image analysis based on iterative region growing using semantics", *IEEE Trans. Geosci. Remote Sensing*, vol. 45, no. 12, pp. 3919-3931, 2007.

[14] Q. Yu and D. A. Clausi, "IRGS: MRF based image segmentation using edge penalties and region growing", *IEEE Trans. Pattern Anal. Machine Intell.* , vol. 30, no. 12, pp. 2126-2139, 2008.

[15] D. A. Clausi, K. Qin, M.S. Chowdhury, P. Yu and P. Maillard, "MAGIC: MAp-Guided Ice Classification" *Canadian Journal of Remote Sensing*, vol. 36, no. 1, pp. S13-S25, 2010.

[16] S.Z. Li, Markov random field modeling in computer vision, Springer, New York, 2001.

[17] D. H. Koekman, M. A. M. Vissers and T. N. Tran, "Unsupervised full-polarimetric SAR data segmentation as a tool for classification of agricultural areas", *IEEE J. Sel. Topics Appl. Earth Obs. Remote Sens.*, vol. 4, no. 2, pp. 402-411, 2011.

[18] J. D. Wegner, R. Hansch, A. Thiele and U. Soergel, "Building detection from one orthophoto and high-resolution InSAR data using conditional random fields", *IEEE J. Sel. Topics Appl. Earth Obs. Remote Sens.*, vol. 4, no. 1, pp. 83-91, 2011.

[19] D. H. Koekman, M. A. M. Vissers and N. Wielaard, "PALSAR wide-area mapping of Borneo: methodology and map validation", *IEEE J. Sel. Topics Appl. Earth Obs. Remote Sens.*, vol. 3, no. 4, pp. 605-617, 2010.

[20] Y. Tarabalka, M. Fauvel, J. Chanussot and J. A. Benediktsson, "SVM- and MRF-based method for accurate classification of hyperspectral images", *IEEE Geosci. Remote Sens. Lett.*, vol. 7, no. 4, pp. 736-740, 2010.

[21] D. Gleich, "Markov random field models for non-quadratic regularization of complex SAR images", *IEEE J. Sel. Topics Appl. Earth Obs. Remote Sens.*, *to appear*, 2012.

[22] Y. Yang, H. Sun and C. He, "Supervised SAR image MPM segmentation based on region-based hierarchical model", *IEEE Geosci. Remote Sens. Lett.*, vol. 3, no. 4, pp. 517-521, 2006.

[23] G. S. Xia, C. He and H. Sun, "Integration of synthetic aperture radar image segmentation method using Markov random field on region adjacency graph", *IET Radar Sonar Navig.,* , vol. 1, no. 5, pp. 348-353,2007.

[24] Y. Li, J. Li and M. A. Chapman, "Segmentation of SAR intensity imagery with a voronoi tessellation, Bayesian inference, and reversible jump MCMC algorithm", *IEEE Trans. Geosci. Remote Sens.*, vol. 48, no. 4, pp. 1872-1881, 2010.

[25] J. W. Modestino and J. Zhang, "A Markov random field model-based approach to image interpretation", *IEEE Trans. Pattern Anal. Mach. Intell.*, vol. 14, no. 6, pp. 606-615, June 1992.

[26] A. Sarkar, M. K. Biswas and K. M. S. Sharma, "A simple unsupervised MRF model based image segmentation approach", *IEEE Trans. Image Processing*, vol. 9, no. 5, pp. 801-812, 2000.

[27] Y. Yu and S. T. Acton, "Speckle reducing anisotropic diffusion", *IEEE Trans. Image Processing*, vol. 11, no. 11, pp. 1260-1270, 2002.

[28] Y. Yu and S. T. Acton, "Edge detection in ultrasound imagery using the instantaneous coefficient of variation", *IEEE Trans. Image Processing*, vol. 13, no. 12, pp. 1640-1655, 2004.

[29] Y. Yu and S. T. Acton, "Automated delineation of coastline from polarimetric SAR imagery", *Int. J. Remote Sensing*, vol. 25, no. 17, pp. 3423-3438, 2004.

[30] P. Perona and J. Malik, "Scale space and edge detection using anisotropic diffusion", *IEEE Trans. Pattern Anal. Mach. Intell.* vol. 12, pp. 629-639, 1990.

[31] L. Vincent and P. Soille, "Watershed in digital spaces: an efficient algorithm based on immersion simulations", *IEEE Trans. Pattern Anal. Mach. Intell.* vol. 13, no. 6, pp. 583-598, June, 1991.

[32] A. C. Bovik, "On detecting edges in speckle imagery," *IEEE Trans. Acoust., Speech, Signal Processing*, vol. 36, pp. 1618–1627, Oct. 1988.

[33] R. Touzi, A. Lopès, and P. Bousquet, "A statistical and geometrical edge detector for SAR images," *IEEE Trans. Geosci. Remote Sensing*, vol. 26, pp. 764–773, Nov. 1988.

[34] R. Fjortoft, A. Lopes, P. Marthon, and E. Cubero-Castan, "An optimal multiedge detector for SAR image segmentation," *IEEE Trans. Geosci. Remote Sensing*, vol. 36, pp. 793–802, May 1998.

[35] J. S. Lee, "Digital image enhancement and noise filtering by use of local statistics", *IEEE Trans. Pattern Anal. Mach. Intell.*, vol. PAMI-2, pp. 165-168, 1980.

[36] A. Lopes, R. Touzi and E. Nezry, "Adaptive speckle filters and Scene heterogeneity", *IEEE Trans. Geosci Remote Sensing*, vol. 28, no. 6, pp. 992-1000, 1990.

[37] J. A. Richards and X. Jia, Remote Sensing Digital Image Analysis: An Introduction, , Springer, Berlin, 2006.

[38] G. Celeux, F. Forbes and N. Peyrard, "EM processing using mean field-like approximations for Markov model-based image segmentation", Research Report RR-4105, INRIA, 2001.